

# Gas Dispersion Coefficient Test System and Dimensionless Inversion Method for Porous Media

Yueping Qin, Mingyan Guo,\* Fengjie Zhang, Zimeng Li, Qiang Liu, and Fei Tang

Cite This: *ACS Omega* 2023, 8, 45137–45151

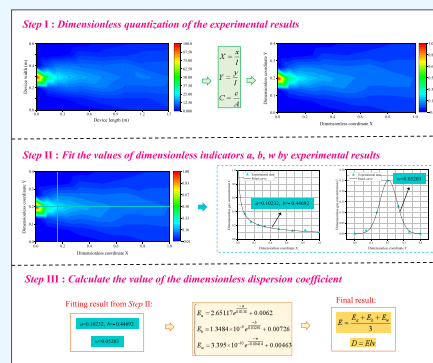
Read Online

ACCESS |

Metrics &amp; More

Article Recommendations

**ABSTRACT:** Due to the complex porous media structure of the longwall gob area, it has been difficult to determine the gas dispersion coefficient of oxygen when studying spontaneous coal combustion in the gob area. In this work, we first designed an experimental device for testing the gas diffusion coefficient of porous media. Then, the distribution law of gas concentration in porous media under different particle size conditions was obtained by experiments. Subsequently, we established a dimensionless mathematical model of gas dispersion in porous media and developed a corresponding numerical simulator based on the finite volume method (FVM). The influence of the dimensionless gas dispersion coefficient on the gas concentration distribution was analyzed, and then a dimensionless inversion method of the gas dispersion coefficient was summarized and put forward. Finally, we obtained the values of the gas dispersion coefficient in the experimental device under different particle size conditions by inversion and discussed its effect on the gas dispersion behavior in porous media. The results show that (1) the distribution of gas concentration obtained from the experimental test and numerical simulation is consistent, which verifies the reliability of our work; (2) the dimensionless gas concentration is the highest near the injection point and gradually decreases along the depth and both sides of the test container; (3) with the increase of the dimensionless gas dispersion coefficient, the distance required for uniform gas mixing in the test container is gradually shortened and the gas dispersion coverage is wider; and (4) the larger pore space facilitates the dispersion behavior of the gas, and the gas dispersion coefficient shows a parabolic trend with the increase of porous medium particle size.



## 1. INTRODUCTION

China is the largest coal producer and consumer in the world, and the share of coal in primary energy consumption has been greater than 50% for a long time.<sup>1–4</sup> As the depth and intensity of coal mining increase, mining conditions have become more and more complex and dangerous.<sup>5–7</sup> Spontaneous coal combustion is one of the most important threats, which mainly occurs in the gob area of longwall mining face.<sup>8,9</sup> The interior of the gob area is full of rocks after the collapse of the roof, forming a complex porous medium structure.<sup>10–12</sup> In addition, a large amount of crushed coal is left in the gob area. The fresh air leaking into the gob area oxidizes with the crushed coal, and the heat released from the reaction gradually accumulates and eventually causes a fire, leading to huge human and property losses.<sup>13,14</sup>

Understanding the mechanism of spontaneous coal combustion in a longwall gob area is the basis of coal mine fire prevention and control.<sup>15,16</sup> In our previous studies, as shown in Figure 1, we have proposed a multifield coupled catastrophic model for spontaneous coal combustion in the gob area of longwall mining face.<sup>17–20</sup> We systematically sorted out the interactions and relations among multiple physical fields that cause spontaneous coal combustion in the gob area and provided some new ideas for related research. However, the

accuracy of numerical calculations depends on the values of various parameters. When the gob oxygen concentration field is calculated, the dispersion coefficient of oxygen is involved. The inaccurate value of the gas dispersion coefficient will lead to the unreliable calculation results.<sup>18,21,22</sup> Therefore, it is of great significance to investigate the gas dispersion flow rule in porous media structure and obtain the accurate gas dispersion coefficient for the study of the spontaneous coal combustion mechanism in the gob area.

In fluid mechanics, dispersion effect is the main characteristic of fluid flow in porous media.<sup>23,24</sup> When the fluid flows, the tracer gradually diffuses outward, continuously occupying a larger and larger flow area, which exceeds the expected occupation area of the average flow, and this propagation phenomenon is called hydrodynamic dispersion in porous media.<sup>25,26</sup> The key to study the fluid dispersion in porous media

Received: October 2, 2023  
Revised: October 24, 2023  
Accepted: October 31, 2023  
Published: November 14, 2023



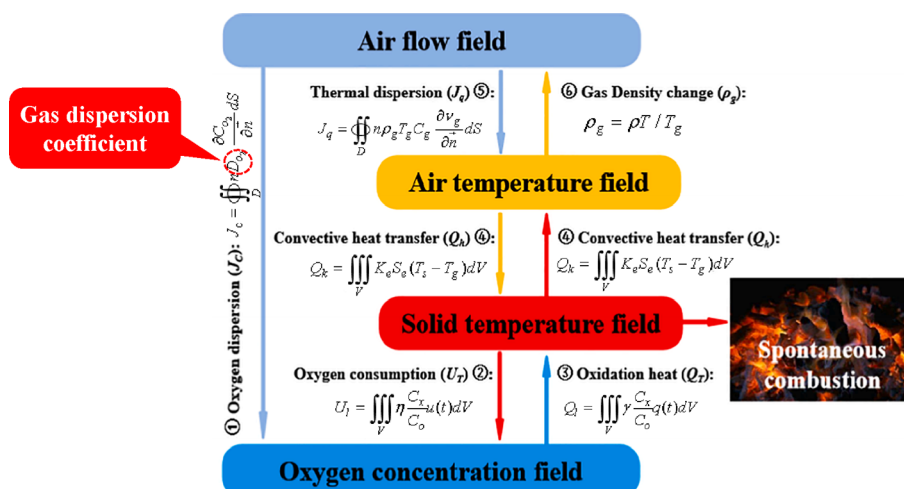


Figure 1. Multifield coupling mechanism of spontaneous coal combustion in the gob area<sup>18</sup>

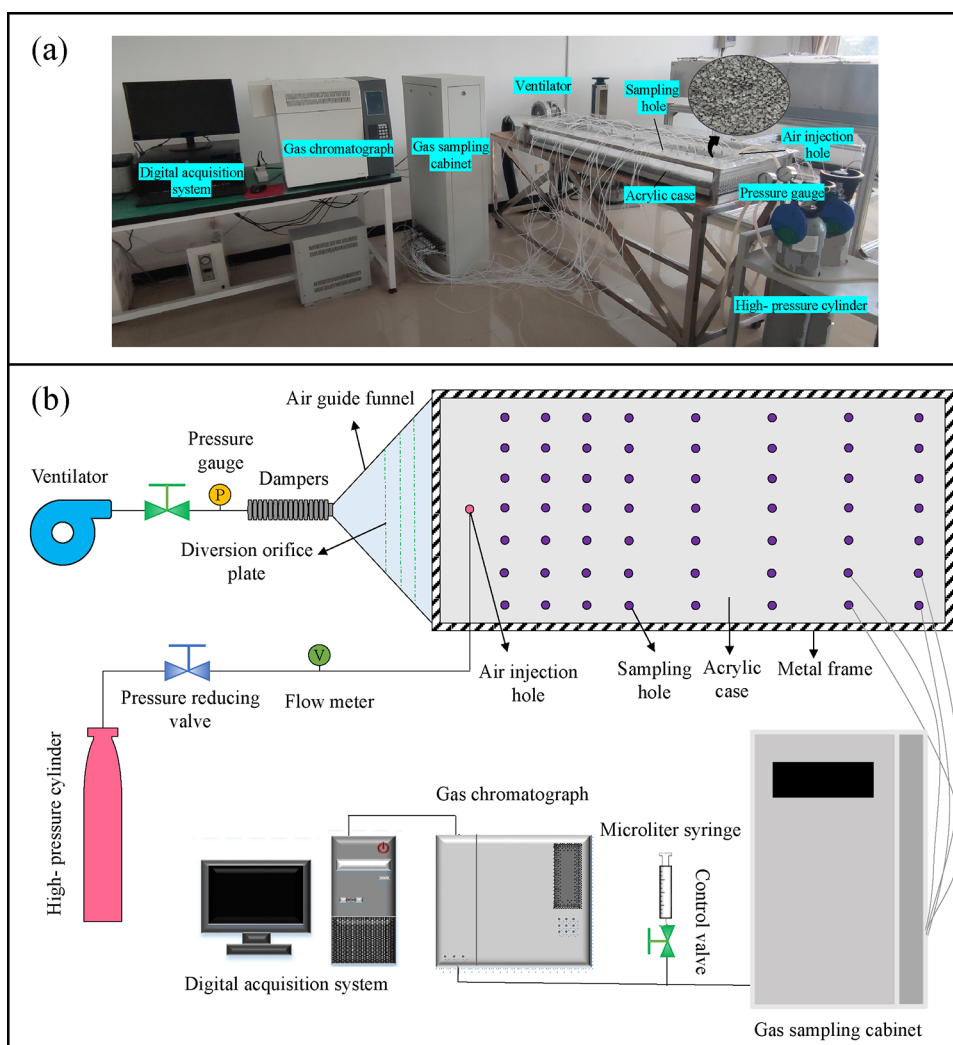


Figure 2. Experimental device diagrams: (a) physical diagram; (b) schematic diagram (note: each sampling hole is connected to the gas collection cabinet; only part of the connection effect is shown here).

is to determine the dispersion coefficient.<sup>27,28</sup> In this regard, many scholars have carried out a large number of related studies through theoretical deduction, numerical simulation, and laboratory testing. Ding et al.<sup>29</sup> established a mathematical

model of one-dimensional flow field dispersion in mine dump and obtained the calculation formula of longitudinal hydrodynamic dispersion coefficient. Zhang et al.<sup>30</sup> conducted a two-dimensional dispersion experiment in the laboratory using a

large-size seepage tank and obtained the longitudinal dispersion coefficient and transverse dispersion coefficient through the experimental results and analytical solutions. Sahimi and Indakm<sup>28</sup> designed a fluid dispersion experiment in two-dimensional porous media and found that the longitudinal dispersion coefficient had no linear relationship with the flow rate. Romero-Gomez et al.<sup>31</sup> got the modified convection–diffusion–reaction transport equation and the calculation formula of axial dispersion coefficient through the dispersion experiment of water flow in laminar flow state. Jiao and Htzl<sup>32</sup> carried out miscible displacement experiments with fluids having density and viscosity differences in a plexiglass column containing uniform and isotropic sand pack. They found that the dispersion coefficient continued to decline when the density difference of the displaced fluid increased or the viscosity ratio decreased. Pugliese and Poulsen<sup>33</sup> used a series of particles with different shapes and sizes as porous media to conduct experimental research on fluid dispersion. The results show that the closer the porous media particles are to the sphere, the more obvious the linear relationship between the dispersion coefficient and water flow velocity is. In summary, most scholars mainly study the dispersion coefficient of liquid, but few study the dispersion coefficient of gas in porous media. However, the gas dispersion coefficient is widely used in engineering technology. The calculation of gas concentration not only provides technical basis for preventing coal spontaneous combustion but also influences the control of gas disaster and the exploitation of coalbed methane.<sup>34,35</sup> Therefore, it is urgent to study the measurement method of the gas dispersion coefficient in porous media.

To solve the above problems, in this work, we studied the test method of the gas dispersion coefficient in porous media by combining numerical simulation and experimental measurement. First, we designed an experimental device for gas dispersion in porous media and measured the gas concentration distribution in the device under different particle size conditions. Subsequently, we established the dimensionless mathematical model of gas dispersion in porous media and prepared a corresponding numerical simulator based on the finite volume method (FVM). Then, the influence of the dimensionless dispersion coefficient on the distribution of gas concentration was analyzed, and an inversion method of the gas dispersion coefficient was summarized and proposed. Finally, according to the experimental results, we obtained the gas dispersion coefficients under different particle size conditions of porous media by inversion and analyzed the influence of particle size on the gas dispersion flow in porous media.

## 2. EXPERIMENTAL SECTION

**2.1. Experimental Device.** In this study, with reference to the one-dimensional porous medium liquid dispersion experimental equipment,<sup>32,36</sup> an experimental device that can perform two-dimensional gas dispersion was designed and developed independently. As shown in Figure 2, this porous media gas dispersion coefficient test device is mainly composed of four parts: ventilation unit, test container, gas injection unit, and sampling analysis unit.

The ventilation unit consists of four parts: a vortex ventilator, three-way valve, pressure gauge, and air guide funnel. The adjustable range of airflow velocity is 0–2 m/s. The vortex ventilator can provide continuous power to the airflow, and the pressure gauge shows the airflow pressure through the test

container. Three diverting orifice plates are arranged in the air guide funnel, which can make the airflow uniform.

The test container is the main body of the experimental device and the place where gas dispersion occurs. It consists of an acrylic box and a metal frame. With reference to previous literature,<sup>24,30</sup> the size of the acrylic box is determined to be 1400 mm × 500 mm × 100 mm and the box is equipped with crushed rock. The top plate of the acrylic box is provided with a gas injection hole and 7 × 8 gas sampling holes, each with a diameter of 1 mm. Considering that the gas concentration near the injection hole changes greatly, the distribution of gas sampling holes in this area is relatively dense. The left and right side walls of the acrylic box are distributed with ventilation mesh holes to ensure that air flows through the test container smoothly.

The gas injection unit is composed of a high-pressure cylinder, a pressure reducing valve, and a flowmeter.<sup>37,38</sup> The CO<sub>2</sub> gas with a small content in air is selected as the index gas. The 8 L CO<sub>2</sub> high-pressure cylinder with a 99.9% concentration is used as the gas source, and the compressed CO<sub>2</sub> in the high-pressure gas cylinder can be safely and stably released by the pressure reducing valve. By controlling the injection pressure equal to the flow pressure, the airflow velocity in the vertical airflow direction can be 0. When the index gas is injected into the test container, the air duct is connected to the gas injection hole by a flower tube (a tubular structure with uniform holes in the side wall). The flower tube makes the air source injected into the container linear, which can reduce the fluctuation of index gas concentration in the height direction of the test container. In addition, the gas injection unit selects the mode of continuous gas injection rather than instantaneous gas injection. With the increase of gas injection time, the gas concentration in the test container will eventually stabilize, so the dispersion of index gas in the test container can be regarded as a two-dimensional steady-state process.

The sampling analysis unit includes a gas sampling cabinet, a microliter syringe, a gas chromatograph, and a digital acquisition system. To ensure the accuracy of sampling, we adopt a combination of manual collection by a microliter syringe and automatic collection by a gas sampling cabinet. The collected gas samples are sent to the gas chromatograph for analysis and then processed by the digital acquisition system to obtain the distribution of CO<sub>2</sub> concentration at each measurement point.

**2.2. Experimental Procedure.** In order to accurately obtain the distribution of the CO<sub>2</sub> concentration in the test container, a two-dimensional gas dispersion experiment in porous medium needs to be carried out according to the following steps:

**Pre-preparation.** Connect the components of the experimental device and seal all gaps with sealant. Then, check whether the connections are well sealed, apply the soapy water to the connections to form a film, start the fan, and observe if the film breaks. Seal all the gas sampling holes with rubber plugs to ensure that there is no air leakage from the gas sampling holes. Finally, use the label paper to number each sampling hole to facilitate the experiment.

**Buried measurement points and filling medium.** According to the location of the gas injection hole and gas sampling hole, arrange the gas injection flower tube and gas sampling flower tube in the corresponding position of the test container and fix with strong glue. Evenly fill the

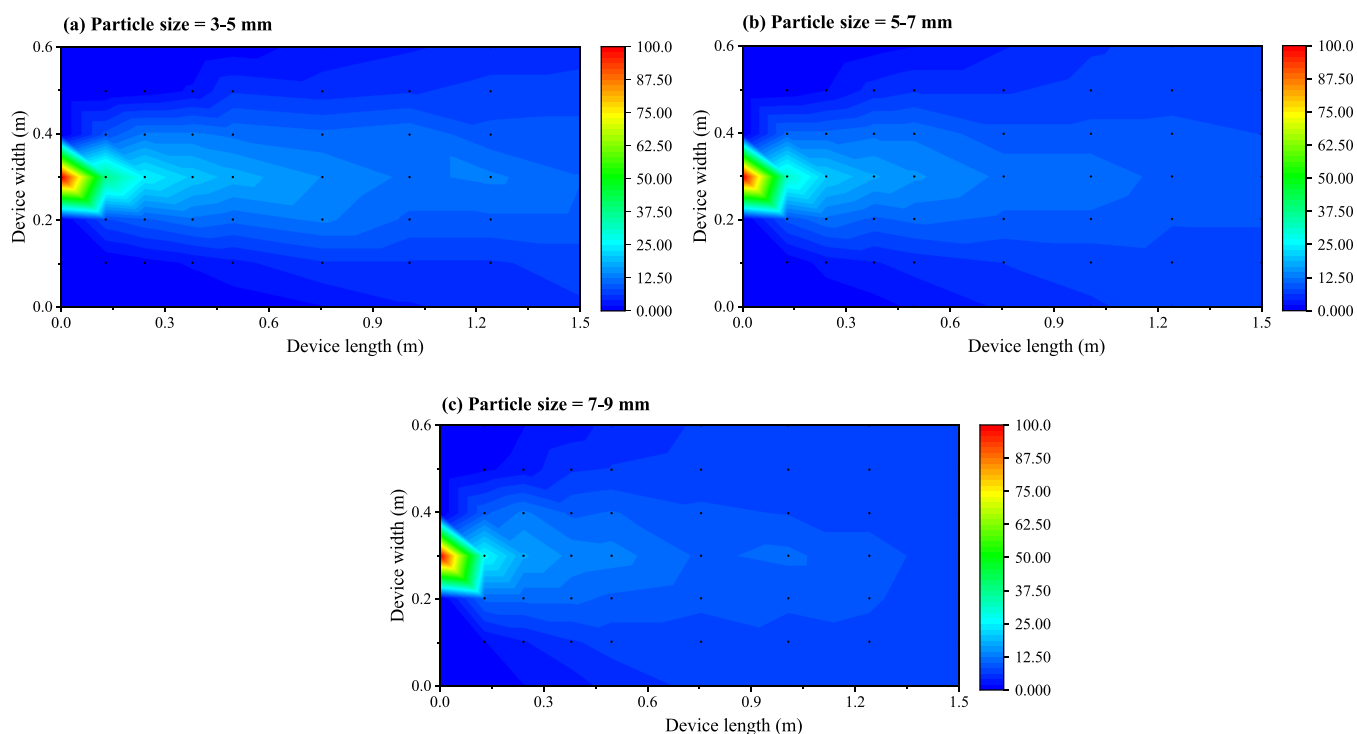


Figure 3. Distribution of the CO<sub>2</sub> concentration in the device under different particle sizes of porous media.

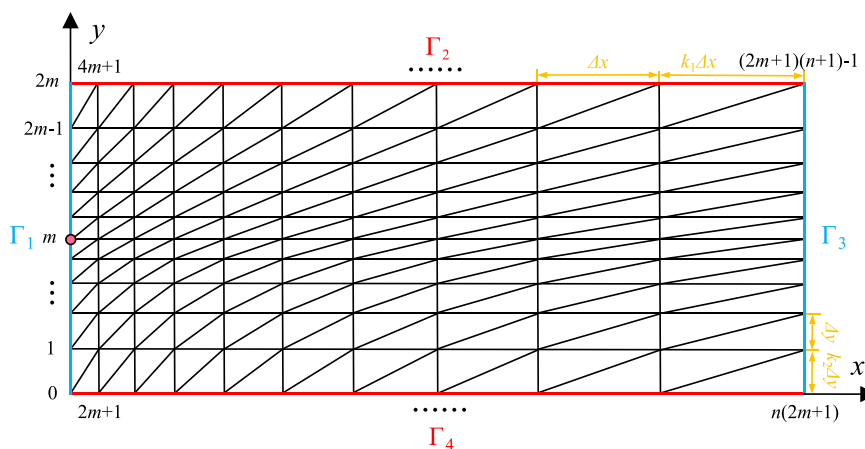


Figure 4. Model solution area and meshing.

porous medium within a certain particle size range into the test container, and fix the cover and seal it with sealant. Ventilation and gas injection. Start the fan and use the control valve to adjust the airflow volume through the test container. Open the high-pressure cylinder and adjust the index gas flow by the reducing valve. Continuously ventilate and inject gas into the test container for 1 h to ensure that the gas concentration in the test container is steady.

Sampling and analysis. When the gas chromatograph is ready, collect the gas sample from any gas sampling hole with a syringe for analysis, and analyze the sample again in the same sampling hole after an interval of 5 min. When the gas concentration measured for two consecutive times is the same, it can be considered that the gas concentration in the test container has reached a steady state. Then, start the automatic sampling system and automatically collect the sample gas from each sampling

point; finally, analyze the extracted sample gas by the gas chromatograph.

**2.3. Experimental Results.** We carried out three sets of experiments when the particle sizes of porous media were 3–5, 5–7, and 7–9 mm, respectively, and the experimental results are shown in Figure 3.

Figure 3 shows the distribution of the CO<sub>2</sub> concentration in the test container under different particle sizes. Due to the limitations in the number of measurement points and test accuracy, the contour of the CO<sub>2</sub> concentration distribution in the container is not smooth enough. The CO<sub>2</sub> concentration data at some measuring points have small fluctuations, but the overall experimental test results still truly reflect the dispersion behavior of the gas inside the device. The results show that with the continuous injection of CO<sub>2</sub> at the gas injection hole, the CO<sub>2</sub> gas was sufficiently dispersed both vertically and horizontally in the test container under the driving force of

airflow. Near the gas injection hole, the CO<sub>2</sub> concentration is the highest. With the increase of the longitudinal dispersion distance, the gas concentration gradually decreases but the gas dispersion range gradually expands on the horizontal. In addition, as the particle size of the porous medium increases, the dispersion coverage of CO<sub>2</sub> in the device also gradually expands.

### 3. MATHEMATICAL MODEL

**3.1. Modeling.** As shown in Figure 4, the rectangular region formed by horizontal projection of the cuboid space on the right side of the injection hole in the test container is selected as the solution area of the gas dispersion model. The length of the solution area is  $l$ , and the width is  $2w$ . Taking the lower-left vertex of the solution area as the coordinate origin, the  $x$ -axis and  $y$ -axis are set along the length direction and width direction of the solution area and a two-dimensional rectangular coordinate system is established. In addition, the model is based on some simplification and assumptions: ① In the design of the test container, its height is much smaller than the length and width, and the adoption of the gas injection flower tube reduces the fluctuation of gas concentration in the direction of container height, so it is assumed that there is no change of gas concentration in the direction of container height. ② The vortex ventilator and high-pressure gas cylinder can provide airflow and index gas in a sustainable and stable manner. After a period of time, the concentration of index gas in the test container tends to a steady state, so the influence of time is no longer considered. ③ The pressure of airflow in the  $y$ -axis direction of the test container is 0, so the airflow velocity in the  $y$ -axis direction of container  $v_y = 0$ . By considering the above conditions, any quadrilateral area element in the solution area is selected. According to the mass conservation law and Fick's law, the change in index gas concentration per unit time equals the quality difference of index gas that flows into and out of the element. Therefore, the two-dimensional steady-state governing equation of gas dispersion in porous media can be established as follows:<sup>32,39,40</sup>

$$\frac{\partial}{\partial x} \left( E_x \frac{\partial c}{\partial x} \right) + \frac{\partial}{\partial y} \left( E_y \frac{\partial c}{\partial y} \right) - \frac{\partial(v_x c)}{\partial x} - \frac{\partial(v_y c)}{\partial y} = 0 \quad (1)$$

where  $c$  is the volume concentration of the index gas in the test container, %;  $E_x$  and  $E_y$  are the gas dispersion coefficients in the  $x$ -axis and  $y$ -axis directions, m<sup>2</sup>/s; and  $v_x$  and  $v_y$  are the airflow velocity in the  $x$ -axis and  $y$ -axis directions, m/s.

Equation 1 can be further simplified as

$$E_x \frac{\partial^2 c}{\partial x^2} + E_y \frac{\partial^2 c}{\partial y^2} - v_x \frac{\partial c}{\partial x} = 0 \quad (2)$$

The model boundary conditions are shown in Figure 4.  $\Gamma_1$  is the first type of boundary condition, and there is almost no index gas in the inlet airflow, so the value of the index gas concentration on  $\Gamma_1$  is 0.  $\Gamma_2$  and  $\Gamma_4$  are the second type of boundary conditions, and the gas diffusive flux in the  $y$ -axis direction is 0.  $\Gamma_3$  is also the second type of boundary condition. It is assumed that when the value of the boundary length  $l$  is large enough, the gas diffusion flux in the  $x$ -axis direction is 0. Therefore, in the calculations, the boundary length  $l$  is first taken to be a sufficiently large value and then the data within the size range of the test container are intercepted from the solution results. The  $m$  on  $\Gamma_1$  is the gas injection point, and its gas concentration is equal to the gas injection concentration  $A$ .

So far, a complete form of the 2D steady-state model for gas dispersion in porous media can be obtained:

$$\begin{cases} E_x \frac{\partial^2 c}{\partial x^2} + E_y \frac{\partial^2 c}{\partial y^2} - v_x \frac{\partial c}{\partial x} = 0 \\ c|_{\Gamma_1} = 0; c_{(0,w)} = A; \frac{\partial c}{\partial y} \Big|_{\Gamma_2, \Gamma_4} = 0; \frac{\partial c}{\partial x} \Big|_{\Gamma_3} = 0 \end{cases} \quad (3)$$

**3.2. Dimensionless Transformation.** Dimensionless is a mathematical method used to study the nature of physical phenomena.<sup>41–43</sup> By setting appropriate dimensionless parameters, the variables in mathematical models can be effectively reduced, which is convenient for the later inversion of the gas dispersion coefficient. As shown in eq 4, we introduce the following dimensionless parameters to dimensionless the gas dispersion model:

$$X = \frac{x}{l}, Y = \frac{y}{l}, C = \frac{c}{A}, E = \frac{E_x}{lv}, \alpha = \frac{E_y}{E_x} \quad (4)$$

where  $X$  is the dimensionless  $x$ -coordinate;  $Y$  is the dimensionless  $y$ -coordinate;  $C$  is the dimensionless gas concentration;  $E$  is the dimensionless gas dispersion coefficient; and  $\alpha$  is the dimensionless dispersion proportionality coefficient.

By substituting these dimensionless parameters into eq 3, the dimensionless gas dispersion model in porous media can be obtained as follows:

$$\begin{cases} E \frac{\partial^2 C}{\partial X^2} + \alpha E \frac{\partial^2 C}{\partial Y^2} - \frac{\partial C}{\partial X} = 0 \\ C|_{\Gamma_1} = 0; C_{(0,w)} = 1; \frac{\partial C}{\partial Y} \Big|_{\Gamma_2, \Gamma_4} = 0; \frac{\partial C}{\partial X} \Big|_{\Gamma_3} = 0 \end{cases} \quad (5)$$

**3.3. Numerical Solution.** The FVM is one of the most popular numerical simulation methods.<sup>44–46</sup> Its basic idea is as follows: The calculation area is first divided into a series of unrepeated grids and elements, and the control area is circled at each grid point. Then, the differential equation is integrated in each control area, and the integral is discretized. Finally, we can establish a linear system of equations with unknown quantities and solve them.

As shown in Figure 4, the solution area of the gas dispersion model is first triangularly meshed. The closer to the gas injection hole, the more drastic the change of gas concentration in the container. Therefore, with the injection hole as the base point, the spacing between adjacent nodes is set to increase proportionally along the positive direction of the  $X$ -axis and the positive and negative direction of the  $Y$ -axis,  $k_1, k_2 > 1$ .

Select any internal node  $q$  in Figure 4 for analysis. As shown in Figure 5, each internal node has six related elements, and the local node numbering of each related element is successively  $i, j, m$  (rotate counterclockwise, and set the node with the smallest overall number as node  $i$ ). The overall node number and local node number of the elements related to node  $q$  are labeled in Figure 5. Each dashed line in Figure 5 is a straight line through the gravity center of each triangular related element, which is parallel to the opposite edge of node  $q$ . The area enclosed by all the dashed lines forms the control area of node  $q$ .

Integrate eq 1 in the control area of node  $q$ :

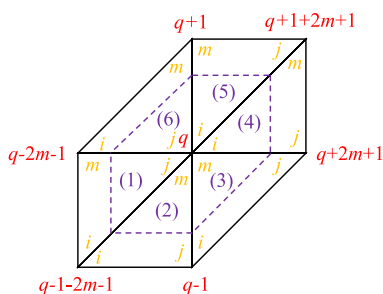


**Figure 5.** Control area and node number of the related elements of internal node  $q$ .

$$\iint_S \left( E \frac{\partial^2 C}{\partial X^2} + \alpha E \frac{\partial^2 C}{\partial Y^2} - \frac{\partial C}{\partial X} \right) dXdY = 0 \quad (6)$$

According to Green's formula, eq 6 can be further simplified to

$$\oint_{\Gamma} C dY - \oint_{\Gamma} \left( E \frac{\partial C}{\partial X} dY - \alpha E \frac{\partial C}{\partial Y} dX \right) = 0 \quad (7)$$

where  $S$  is the area of the node control area;  $\Gamma$  is the perimeter of the control area.

The control area of each node is composed of six related triangular control elements, so the integral (eq 7) can be discretized as follows:

$$\sum_{k=1}^n M_{lk} = \sum_{k=1}^n \left[ C \Delta Y_{lk} - E \frac{\partial C}{\partial X} \Delta Y_{lk} + \alpha E \frac{\partial C}{\partial Y} \Delta X_{lk} \right] = 0 \quad (8)$$

where  $\Delta Y_{lk}$  and  $\Delta X_{lk}$  are the projected lengths on the  $Y$ -axis and  $X$ -axis of the  $k$ th triangular element on the boundary of control area, respectively;  $M_{lk}$  is the contribution of the  $k$ th triangular element composing the control area to node  $q$ .

In any triangular element of the solution area, based on the principle of linear interpolation, the dimensionless gas concentration at any point in the element can be expressed as a function of node coordinates, node gas concentration, and element area:<sup>42,45</sup>

$$C = \frac{1}{2S} [(a_i + b_i X + d_i Y) C_i + (a_j + b_j X + d_j Y) C_j + (a_m + b_m X + d_m Y) C_m] \quad (9)$$

where

$$a_i = X_j Y_m - X_m Y_j, b_i = Y_j - Y_m, d_i = X_m - X_j,$$

$$a_j = X_m Y_i - X_i Y_m, b_j = Y_m - Y_i, d_j = X_i - X_m,$$

$$a_m = X_i Y_j - X_j Y_i, b_m =$$

$$= Y_i - Y_j, d_m =$$

$$= X_j - X_i, S =$$

$$= (b_i d_j - b_j d_i) / 2$$

Taking the  $k$ th triangular element as an example and analyze its contribution to the three nodes  $i, j$ , and  $m$ . First, for node  $m$ , the contribution  $M_{mk}$  of the  $k$ th triangular element to node  $m$  can be obtained by substituting eq 9 into eq 8:

$$\begin{aligned} M_{mk} &= C \Delta Y_k - E \frac{\partial C}{\partial X} \Delta Y_k + \alpha E \frac{\partial C}{\partial Y} \Delta X_k \\ &= \left( \frac{2b_m}{9} - \frac{Eb_i b_m + \alpha E d_i d_m}{3s} \right) C_i \\ &\quad + \left( \frac{2b_m}{9} - \frac{Eb_j b_m + \alpha E d_j d_m}{3s} \right) C_j \\ &\quad + \left( \frac{2b_m}{9} - \frac{Eb_m b_m + \alpha E d_m d_m}{3s} \right) C_m \end{aligned} \quad (10)$$

Similarly, the contribution  $M_{ik}$ ,  $M_{jk}$  of the  $k$ th triangular element to nodes  $i, j$  can be obtained and written in matrix form:

$$\begin{pmatrix} M_{ik} \\ M_{jk} \\ M_{mk} \end{pmatrix} = \begin{pmatrix} k_{ii} & k_{ij} & k_{im} \\ k_{ji} & k_{jj} & k_{jm} \\ k_{mi} & k_{mj} & k_{mm} \end{pmatrix} \begin{pmatrix} C_i \\ C_j \\ C_m \end{pmatrix} \quad (11)$$

where

$$k_{ln} = \left[ \frac{2b_l}{9} - \frac{1}{3s} (Eb_l b_n + \alpha E d_l d_n) \right] (l, n = i, j, m)$$

The treatment of discrete equations for the boundary nodes is consistent with those of the internal nodes and will not be repeated. Search within the solution area and superimpose the contributions of all triangle elements at the same node to synthesize the overall form of the mass conservation equation at each node, and finally a system of linear equations composed of all the nodes is established, as shown in eq 12:

$$\begin{pmatrix} k_{00} & k_{01} & k_{02} & \cdots & k_{0,n-1} & k_{0n} \\ k_{10} & k_{11} & k_{12} & \cdots & k_{1,n-1} & k_{1n} \\ k_{20} & k_{21} & k_{22} & \cdots & k_{2,n-1} & k_{2n} \\ \vdots & \vdots & \vdots & \ddots & \vdots & \vdots \\ k_{n-1,0} & k_{n-1,1} & k_{n-1,2} & \cdots & k_{n-1,n-1} & k_{n-1,n} \\ k_{n0} & k_{n1} & k_{n2} & \cdots & k_{n,n-1} & k_{nn} \end{pmatrix} \begin{pmatrix} C_0 \\ C_1 \\ C_2 \\ \vdots \\ C_{n-1} \\ C_n \end{pmatrix} = \begin{pmatrix} q_0 \\ q_1 \\ q_2 \\ \vdots \\ q_{n-1} \\ q_n \end{pmatrix} \quad (12)$$

where  $C_0, C_1, \dots, C_n$  is the gas concentration at each node;  $k_{00}, k_{01}, \dots, k_{nn}$  are the coefficients of the linear equations; and  $q_0, q_1, \dots, q_n$  are the constants.

Finally, we independently developed a numerical simulator based on the *Visual Studio* programming platform. In this way, according to different models and different needs, codes can be written flexibly to carry out numerical simulation. The programming process is listed in Figure 6. First, the constants, variables, and arrays required for calculation are defined, and the calculation area is divided into grids and nodes. Subsequently, the coefficient matrices of all nodes are assigned sequentially to establish a system of linear equations with the gas concentration as the unknown quantity. Finally, the Gauss–Seidel iterative

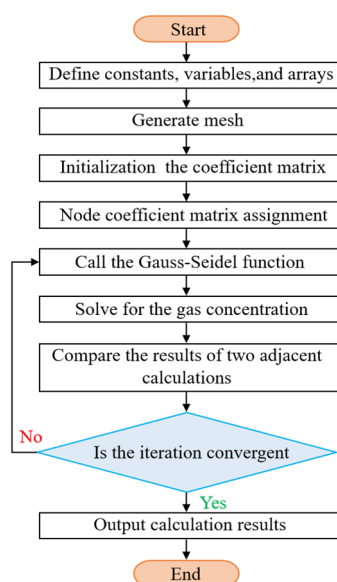


Figure 6. Programming progress.

method is applied to solve the linear equations until the calculation results meet the accuracy requirements, and all the results are output.<sup>47</sup>

## 4. SIMULATION RESULTS AND ANALYSIS

### 4.1. Dimensionless Gas Concentration Distribution.

The specific simulation parameters involved in solving the model are listed in Table 1. These parameters from Table 1 are incorporated into the solution program to simulate gas dispersion laws in porous media.

There are only two undetermined coefficients in the dimensionless gas dispersion model: the dimensionless dispersion coefficient  $E$  and the dimensionless dispersion proportionality coefficient  $\alpha$ , where the  $\alpha$  is the ratio of the longitudinal and transverse gas dispersion coefficient. In the test experiments designed in this work, the particle size of the porous medium is uniformly distributed throughout the device; therefore, here we approximate the value of  $\alpha$  to be 1. By changing the value of the dimensionless dispersion coefficient  $E$ , we can obtain different simulation results and obtain the distribution law of the gas dimensionless concentration in the test container.

Figure 7 shows the distribution of the CO<sub>2</sub> dimensionless concentration inside the test container with different dimensionless dispersion coefficients. The results show that the dimensionless gas concentration is the highest near the gas injection point. From the gas injection point, the dimensionless gas concentration gradually decreases along the depth and both sides of the test container. With the increase in the dimensionless dispersion coefficient, the gas disperses more fully in the  $Y$ -axis direction of the test container, and the dispersion coverage in the test container gradually expands. Taking the dimensionless gas concentration contour  $C = 0.2$  as

an example, it can be found that the whole contour is close to the ellipse. As the dimensionless dispersion coefficient increases, the long axis of the ellipse is gradually shortened, which indicates that the distance required for uniform gas mixing in the test container is gradually shortened and the occurrence of gas dispersion behavior becomes easier.

**4.2. The Relationship between Dimensionless Dispersion Coefficient and Gas Concentration.** In order to quantitatively analyze the relationship between dimensionless dispersion coefficient  $E$  and dimensionless gas concentration distribution, two characteristic lines  $Y = 0.2$  and  $X = 0.161$  were selected according to the change rule of gas concentration in Figure 7.  $Y = 0.2$  is the center line of the  $Y$ -axis, and  $X = 0.161$  is the  $X$ -coordinate value of sampling holes closest to the injection holes in the device. According to the distribution of gas concentration data on the characteristic lines, the variation law of gas concentration with dimensionless coordinates is fitted.

Figure 8 shows the CO<sub>2</sub> dimensionless concentration distribution on the characteristic line  $Y = 0.2$  with different dimensionless dispersion coefficients. It can be found that the gas dimensionless concentration varies drastically along the  $X$ -axis. The gas dimensionless concentration is the highest at the injection point, and then the gas concentration decreases rapidly and tends to stabilize, which is even more drastic with an increase in the dimensionless dispersion coefficient. The simulation data of the dimensionless gas concentration on  $Y = 0.2$  with different dimensionless gas dispersion coefficients were fitted, and the fit goodness  $R^2$  of the obtained fitting curves were all above 0.95. Therefore, the dimensionless gas concentration simulation data change with the  $X$ -axis as follows:

$$C = aX^b \quad (13)$$

where  $a$ ,  $b$  is the undetermined parameter of the fitting curve.

Figure 9 shows the dimensionless CO<sub>2</sub> concentration distribution on the characteristic line  $X = 0.161$  with different dimensionless dispersion coefficients. The results show that the change rule of dimensionless gas concentration with the  $Y$ -axis is similar to a normal distribution. At  $Y = 0.2$ , the gas concentration reaches its peak, and on both sides of the peak, the gas concentration gradually decreases and falls to the lowest point at the boundary. With the increase of the dimensionless dispersion coefficient, CO<sub>2</sub> is more fully dispersed in the container. The gas concentration distribution is more uniform on the  $Y$ -axis, showing that the peak value of dimensionless gas concentration gradually decreases but the minimum value increases significantly. Under different dimensionless gas dispersion coefficients, the goodness of each fitting curve  $R^2$  is above 0.99 and the variation law of the simulated value on the characteristic line  $X = 0.161$  along the  $Y$ -axis can be obtained:

$$C = C_0 + De^{-(Y-Y_c)^2/2w^2} \quad (14)$$

where  $C_0$  is the minimum value of dimensionless gas concentration;  $D$  is the difference between the peak and the minimum value of dimensionless gas concentration;  $Y_c$  is the  $Y$

Table 1. Numerical Simulation Parameter Values

parameter	length of solution area $l$ (m)	width of solution area $2w$ (m)	dimensionless length of the solution area	dimensionless width of the solution area	gas injection concentration $A$ (%)	dimensionless gas injection concentration	airflow velocity $v_x$ (m/s)
value	1.5	0.6	1	0.4	99.9%	1	0.18

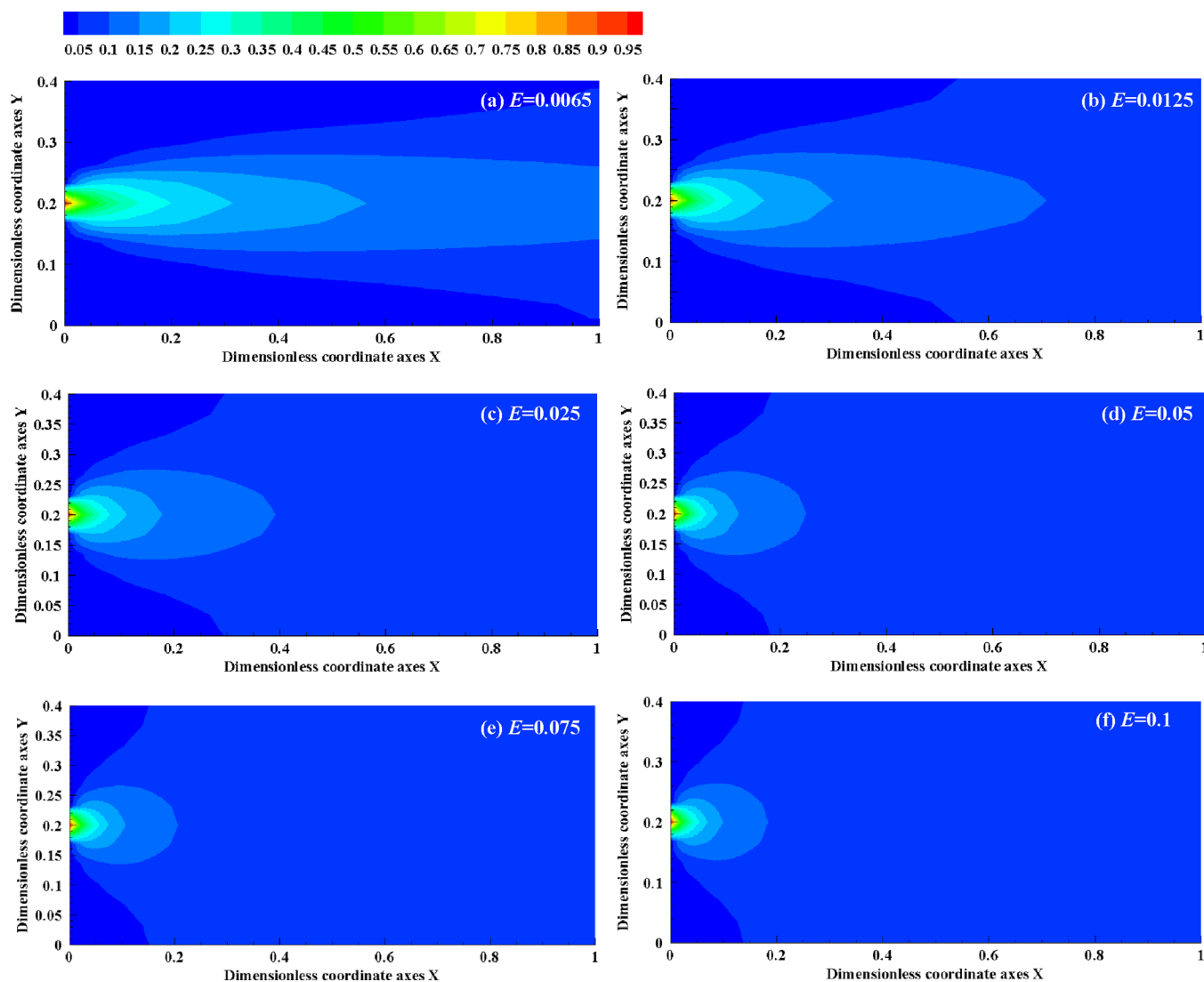


**Figure 7.** Dimensionless concentration distribution of CO<sub>2</sub> with different dimensionless dispersion coefficients.

coordinate value of the peak,  $Y_c = 0.2$ ;  $w$  is the undetermined parameter of the fitting curve.

There is a one-to-one correspondence between different dimensionless dispersion coefficients and different dimensionless gas concentration distribution curve equations. Therefore, we can determine the values of three undetermined parameters  $a$ ,  $b$ , and  $w$  under different dimensionless dispersion coefficients. As shown in Figure 10, the correlation equations between dimensionless gas dispersion characteristic coefficient and undetermined parameters  $a$ ,  $b$ , and  $w$  can be determined by fitting as follows:

$$\begin{cases} E_a = 2.65117e^{-a/0.0138} + 0.0062, R^2 = 0.93739 \\ E_b = 1.3484 \times 10^{-9}e^{-b/0.03291} + 0.00726, R^2 = 0.98863 \\ E_w = 3.395 \times 10^{-10}e^{-w/-0.00414} + 0.00463, R^2 = 0.87181 \end{cases} \quad (15)$$

where  $E_a$ ,  $E_b$ , and  $E_w$  are the dimensionless dispersion characteristic coefficients associated with undetermined parameters  $a$ ,  $b$ , and  $w$ , respectively.

Here, we further define these three undetermined parameters  $a$ ,  $b$ , and  $w$  as the dimensionless index coefficients for gas dispersion coefficient inversion. Through eq 15, we can quickly calculate the value of the dimensionless gas dispersion coefficient from the dimensionless index coefficient.

## 5. INVERSION AND DISCUSSION

**5.1. Gas Dispersion Coefficient Inversion Process.** The process of solving specific parameters in the equation according to the results is called the parameter inversion method.<sup>48,49</sup> In the experiment of gas dispersion in porous media, the distribution of gas concentration is affected by the gas dispersion coefficient, airflow velocity, gas injection concentration, and experiment device size. However, by establishing a simplified dimensionless mathematical model of gas dispersion, we found that the distribution of dimensionless gas concentration is only related to the dimensionless dispersion coefficient  $E$  and the size of solution area. Therefore, when the size of the solution area is fixed, the dimensionless gas concentration distribution will only be affected by the dimensionless dispersion coefficient  $E$ , and the two correspond one by one. By fitting the dimensionless gas concentration distribution on the characteristic lines, we summarized three dimensionless index coefficients  $a$ ,  $b$ , and  $w$

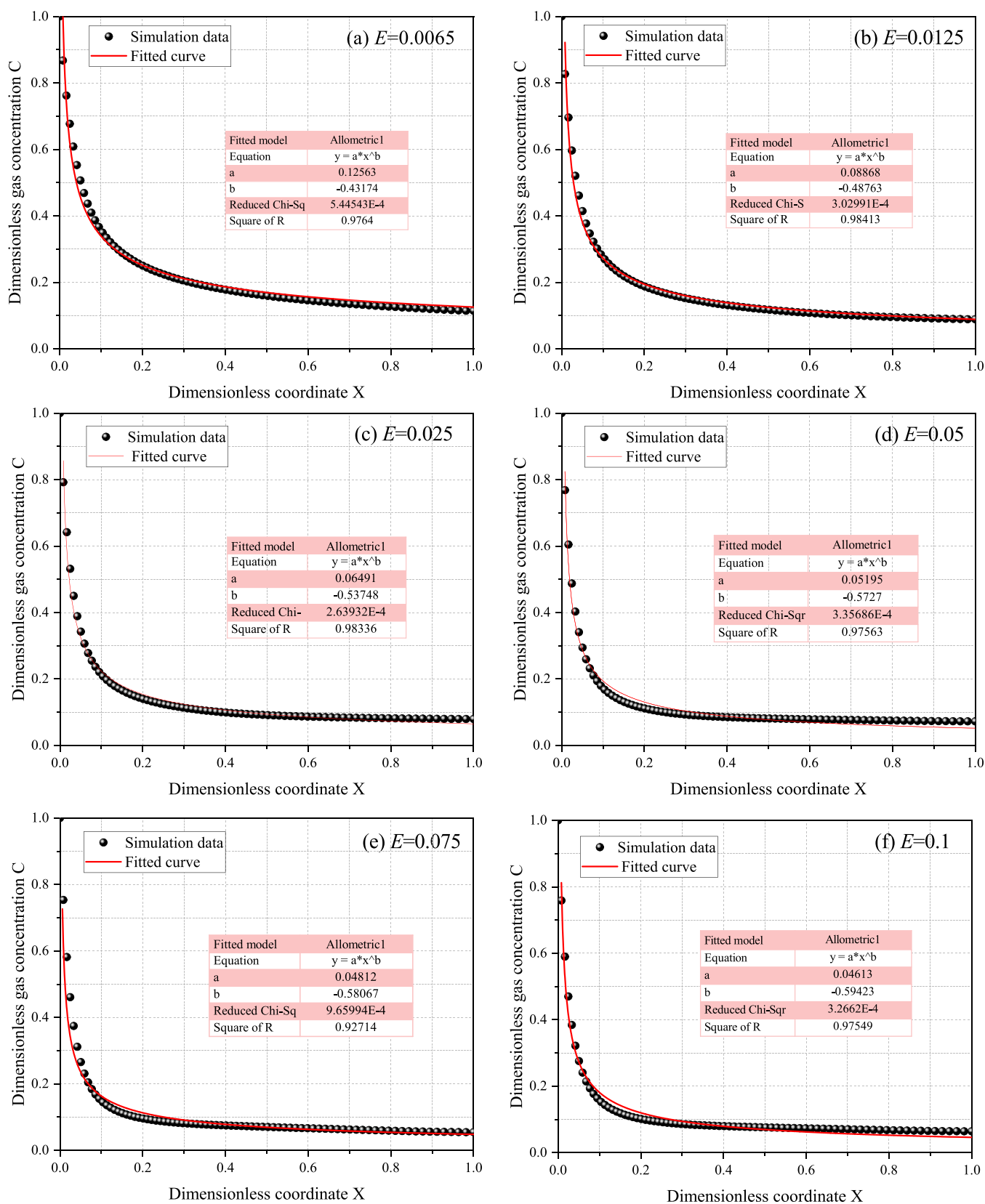


Figure 8. Dimensionless CO<sub>2</sub> concentration distribution on  $Y = 0.2$  with different dimensionless dispersion coefficients.

related to gas dispersion coefficient inversion and determined the functional relationship between each dimensionless index coefficient and dimensionless dispersion coefficient. In this way, we can invert the dimensionless gas dispersion coefficient in the

device through the experimental results of gas concentration distribution. The above is the basic principle of gas dispersion coefficient inversion in porous media.

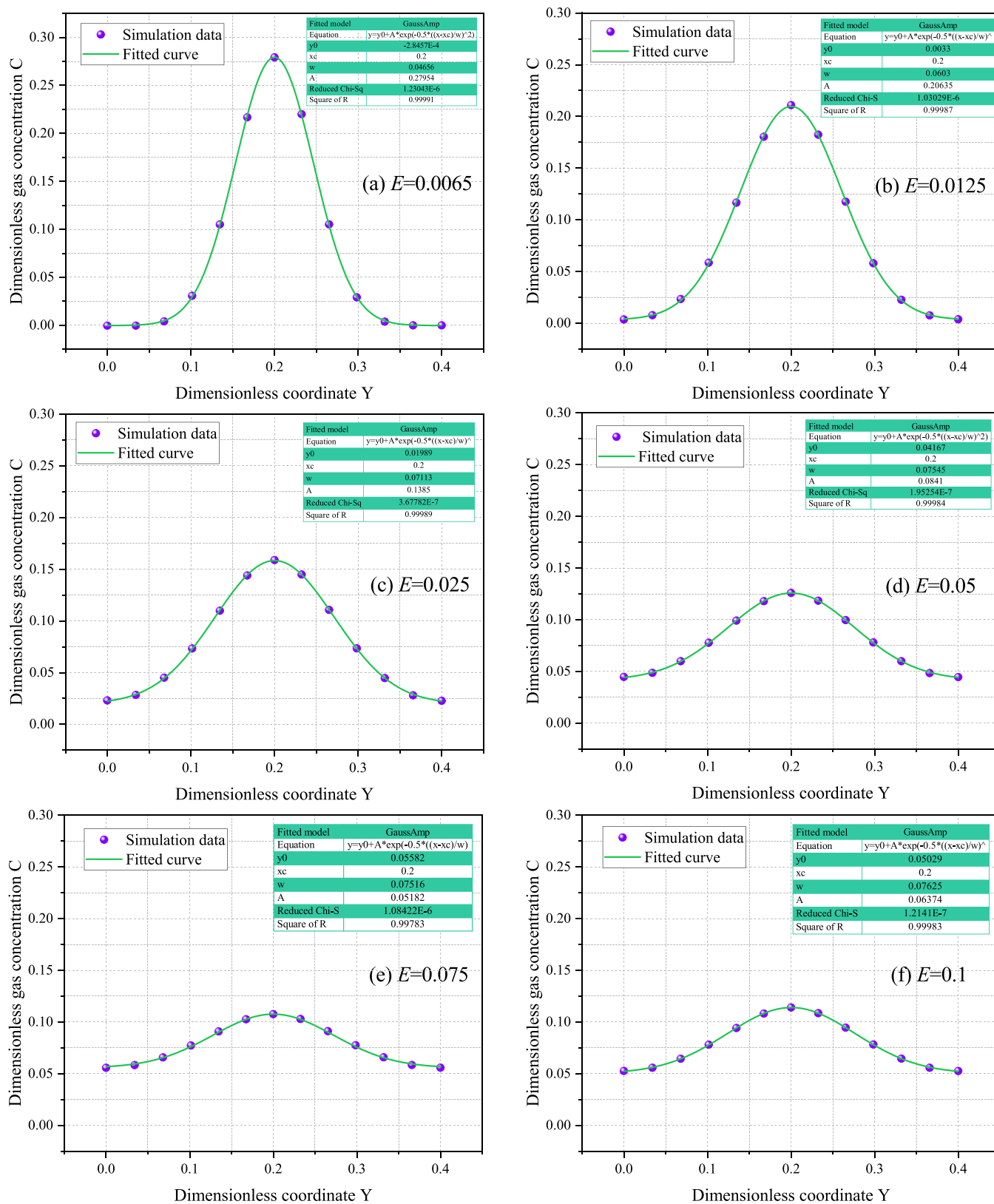
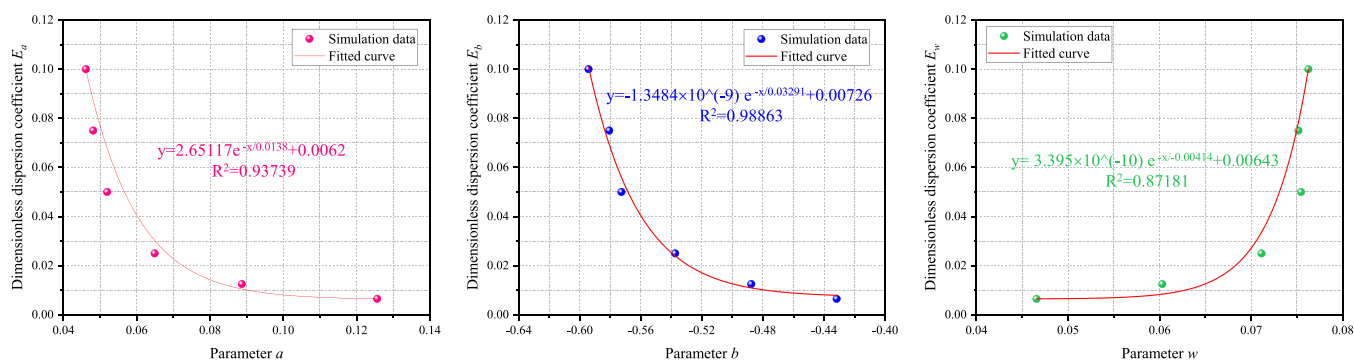


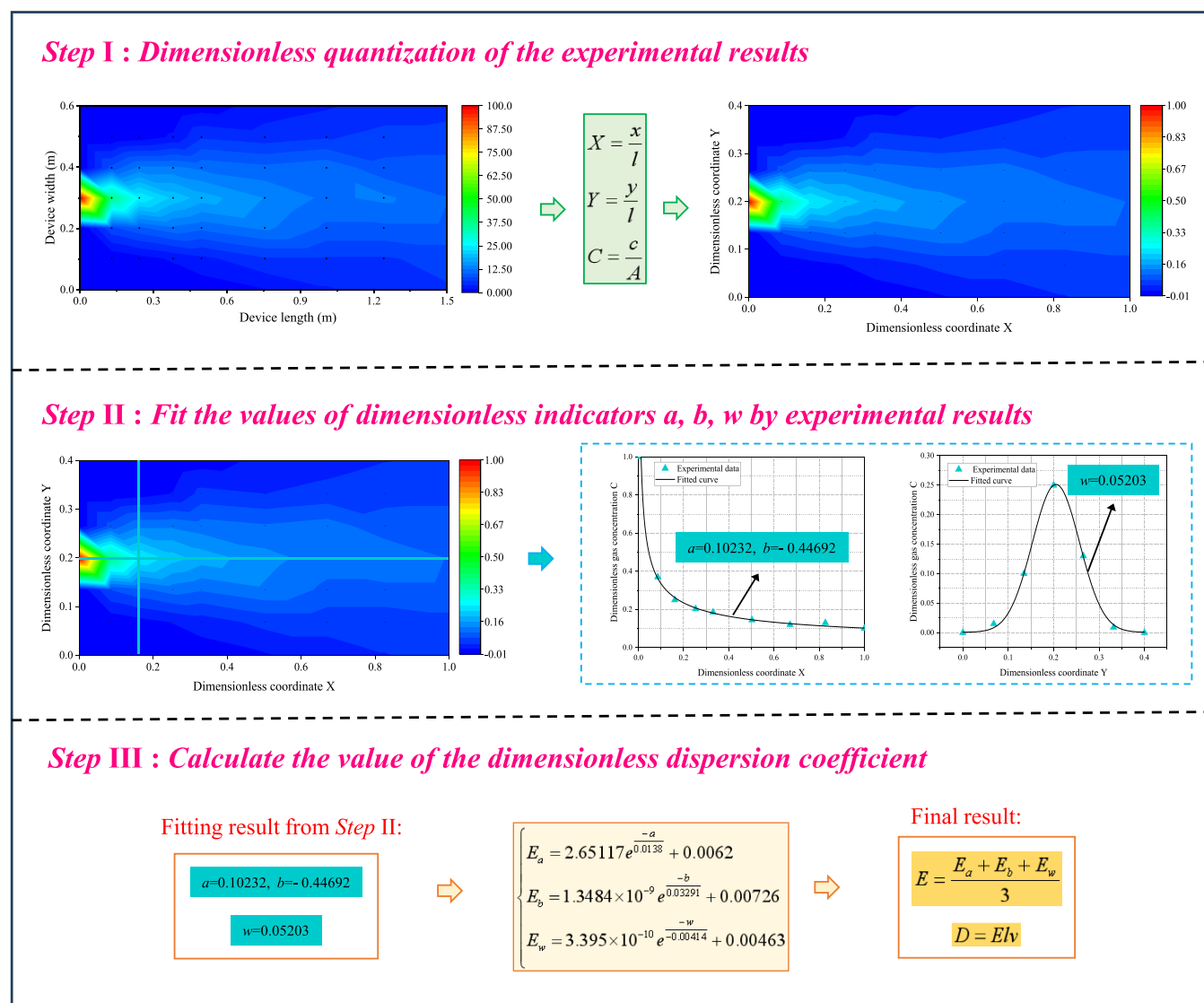
Figure 9. Dimensionless CO<sub>2</sub> concentration distribution on  $X = 0.161$  with different dimensionless dispersion coefficients.

Figure 11 shows the detailed procedure for the inversion of the dimensionless gas dispersion coefficients. First, the gas concentration data obtained by experiment and the coordinates corresponding to each gas sampling hole are dimensionless quantization. Subsequently, the dimensionless gas concentra-

tion distribution data on the characteristic lines  $Y = 0.2$  and  $X = 0.161$  of the experimental data were fitted, and the values of three dimensionless index coefficients  $a$ ,  $b$ , and  $w$  could be obtained. Finally, according to eq 15, the value of the dimensionless gas dispersion coefficient can be calculated.



**Figure 10.** Fitting relationship between dimensionless dispersion coefficient and undetermined parameter  $a$ ,  $b$ , and  $w$ .



**Figure 11.** Dimensionless gas dispersion coefficient inversion process.

Figure 12 shows the experimental data and fitting results of the gas concentration distribution after dimensionless quantization. It can be found that under different particle size conditions, the gas concentration data obtained by experiments also conforms to the fitting eqs 13 and 14, which verify the unity of the experimental results and the numerical simulation results.

Taking the fitting results of gas concentration distribution when the particle size is 3–5 mm in Figure 12a as an example,

the value of dimensionless index coefficients  $a$ ,  $b$ , and  $w$  can be obtained, which are 0.10232,  $-0.51584$ , and 0.05203, respectively. By substituting the above three index values into eq 15, the values of  $E_a$ ,  $E_b$ , and  $E_w$  can be determined as 0.007797, 0.008325, and 0.006698. Next, take the mean of the three dimensionless dispersion characteristic coefficients  $E_a$ ,  $E_b$ , and  $E_w$  to obtain the final calculation result of the dimensionless gas dispersion coefficient:

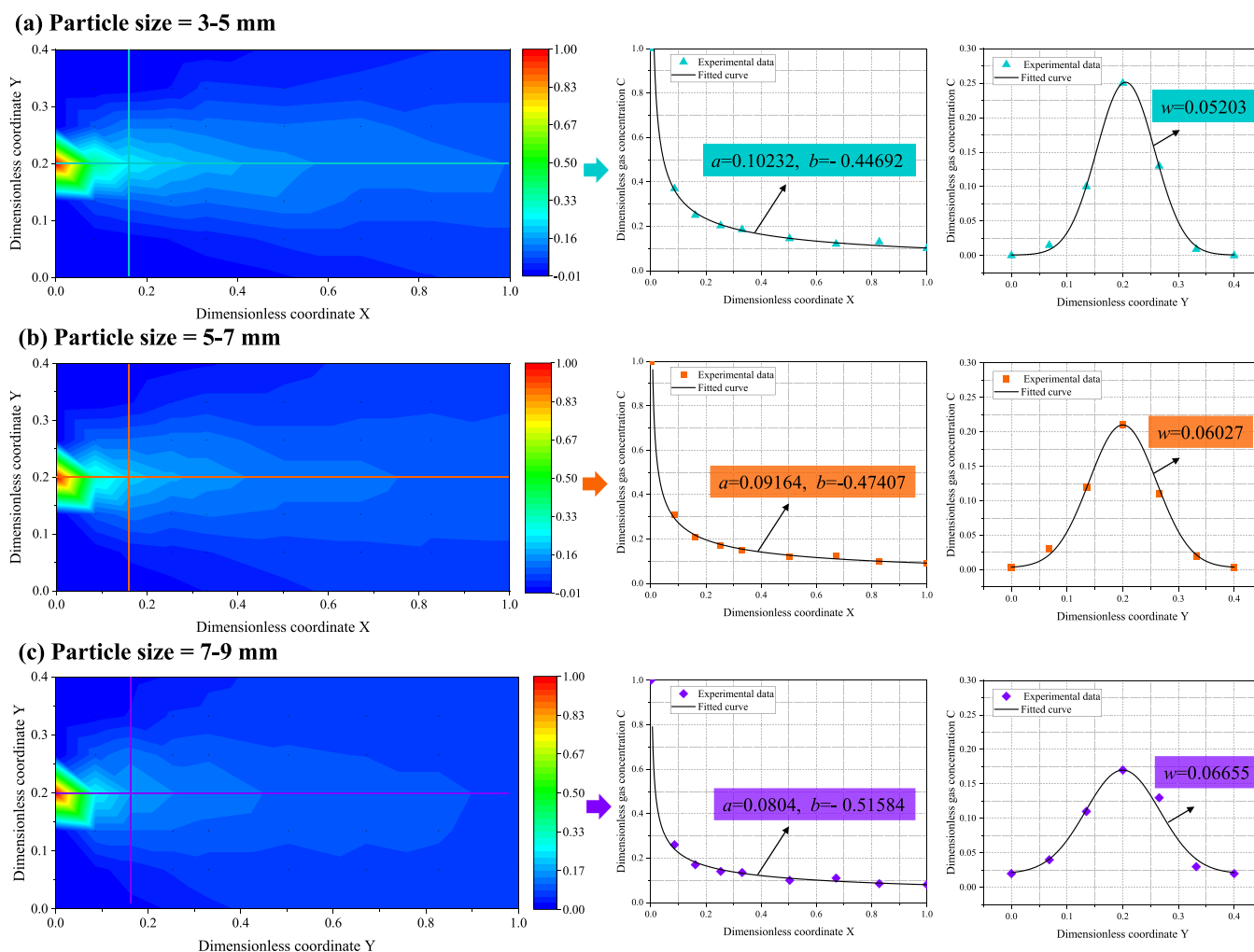


**Figure 12.** Experimental data and fitting results of dimensionless gas concentration distribution under different particle size conditions.

$$E = \frac{E_a + E_b + E_w}{3} \quad (16)$$

Therefore, it is determined that when the particle size of porous medium is 3–5 mm, the value of dimensionless gas dispersion coefficient  $E$  in the experimental device is 0.007607. The conversion relationship between the gas dispersion coefficient  $D$  in porous media and the dimensionless gas dispersion coefficient  $E$  is as follows:

$$D = Elv \quad (17)$$

Substituting the values of  $l$ ,  $v$ , and  $E$  into eq 17, we could finally get the value of gas dispersion coefficient  $D$  is 0.002054 when the particle size of porous medium is 3–5 mm. Similarly, by repeating the above inversion process, it can be obtained that when the particle size of porous medium is 5–7 and 7–9 mm, the value of the gas dispersion coefficient  $D$  in porous medium is 0.002497 and 0.004077, respectively.

**5.2. Effect of Particle Size on Gas Dispersion Coefficient.** In the previous section, by inverting the gas dispersion coefficient in porous medium, as shown in Figure 13, we obtained the values of gas dispersion coefficient inside the experimental device when the particle sizes were 3–5, 5–7, and 7–9 mm. Fitting the variation rule of the gas dispersion coefficient with the average particle size, the results show that the gas dispersion coefficient shows a parabolic trend growth

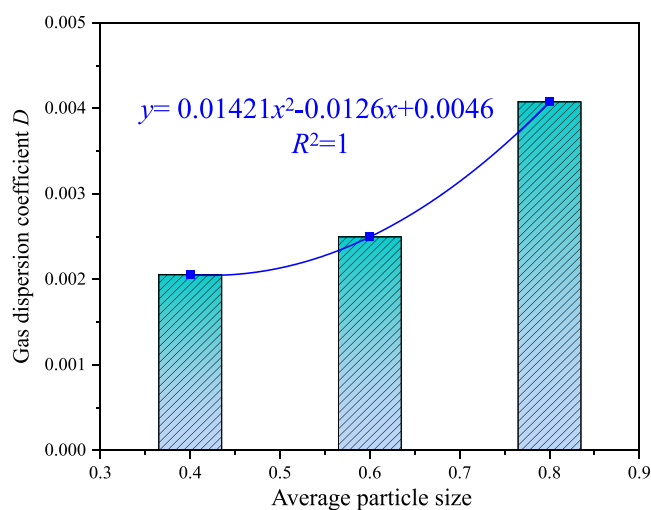


**Figure 13.** Gas dispersion coefficients in porous media under different particle size conditions.

with the increase of particle size of the porous medium. Combining it with Figure 14 can better help us to understand the reasons for this phenomenon. On the one hand, the increase of the porous medium particle size significantly increases its internal porosity. Through the drainage method, we also

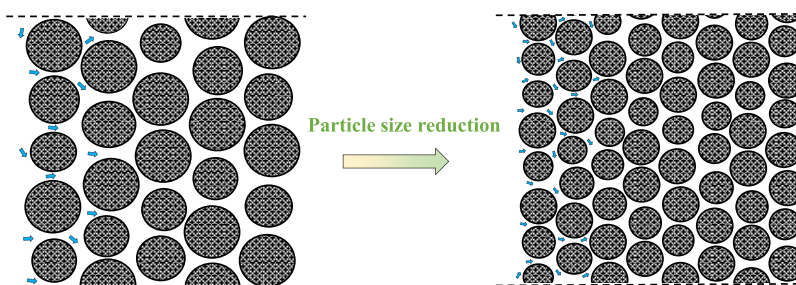


**Figure 14.** Gas dispersion processes under different particle size conditions.

measured the internal porosity of the porous medium under different particle size conditions. When the particle sizes are 3–5, 5–7, and 7–9 mm, the corresponding porosities are 38.87, 40.81, and 43.2%, respectively. Larger pores obviously favor the dispersion behavior of gas. On the other hand, the smaller the particle size of the porous medium, the more difficult the dispersion flow of gas in the porous medium, and the similar the distance of flow, the more complex the tortuous path of gas, which also inhibits the dispersion behavior of gas in the small particle size porous medium.

## 6. CONCLUSIONS

In this paper, we study the gas dispersion law and determine the gas dispersion coefficient in porous media. We first designed an experimental device for testing the gas dispersion coefficient in porous media and carried out the gas dispersion experiments under different particle size conditions. Subsequently, a dimensionless mathematical model reflecting the gas dispersion behavior in the experimental device was established, and a numerical simulator was programmed based on the FVM. Through the numerical simulation results, we analyzed the effect of the dimensionless dispersion coefficient on dimensionless gas concentration distribution and proposed an inversion method of the gas dispersion coefficient. Finally, we obtained the gas dispersion coefficients under different particle size conditions and analyzed the effect of the particle size on the gas dispersion behavior in porous media. The following conclusions are obtained:

The distribution law of gas concentration in the test container obtained from the experimental test and numerical simulation is consistent, and the reliability of the experimental system and mathematical model developed in this paper is verified by mutual corroboration, which can provide help for the study of gas dispersion flow law in porous media.

The dimensionless gas concentration near the gas injection point is the highest. From the gas injection point, the dimensionless gas concentration gradually decreases along the depth and both sides of the test container. With the increase of the dimensionless dispersion coefficient, the distance required for uniform gas mixing in the test container is gradually shortened and the gas dispersion coverage is wider.

The proposed inversion method can quickly determine the gas dispersion coefficient in porous media under different experimental conditions. With the increase of porous medium particle size, the gas dispersion coefficient shows a parabolic trend and the increase of pores is conducive to the gas dispersion behavior in porous media.

## AUTHOR INFORMATION

### Corresponding Author

**Mingyan Guo** – School of Emergency Management and Safety Engineering, China University of Mining & Technology, Beijing, Beijing 100083, PR China; [orcid.org/0009-0001-4346-0424](https://orcid.org/0009-0001-4346-0424); Email: [guomingyan215@163.com](mailto:guomingyan215@163.com)

### Authors

**Yueping Qin** – School of Emergency Management and Safety Engineering, China University of Mining & Technology, Beijing, Beijing 100083, PR China; [orcid.org/0000-0003-0904-4379](https://orcid.org/0000-0003-0904-4379)

**Fengjie Zhang** – School of Emergency Management and Safety Engineering, China University of Mining & Technology, Beijing, Beijing 100083, PR China; [orcid.org/0000-0001-7580-6410](https://orcid.org/0000-0001-7580-6410)

**Zimeng Li** – School of Emergency Management and Safety Engineering, China University of Mining & Technology, Beijing, Beijing 100083, PR China

**Qiang Liu** – School of Emergency Management and Safety Engineering, China University of Mining & Technology, Beijing, Beijing 100083, PR China

**Fei Tang** – School of Emergency Management and Safety Engineering, China University of Mining & Technology, Beijing, Beijing 100083, PR China

Complete contact information is available at:

<https://pubs.acs.org/10.1021/acsomega.3c07628>

### Author Contributions

YQ: supervision, methodology, project administration, writing—review and editing; MG: investigation, methodology, laboratory test, software, writing—original draft; FZ: supervision, project administration, writing—review and editing, proofreader; ZL: investigation, methodology, visualization; QL: software, laboratory test. FT: proofreader.

### Notes

The authors declare no competing financial interest.

## ACKNOWLEDGMENTS

This work was supported by the National Natural Science Foundation of China [grant numbers 52074303 and 51874315].

## REFERENCES

- (1) Zhu, H.; Liao, Q.; Qu, B.; Hu, L.; Wang, H.; Gao, R.; Fang, S.; Zhang, Q. Influence of particle diameter on the scattering characteristics of pre-oxidized coal in THz band. *Colloids Surf., A* **2022**, *646*. DOI: 129006.
- (2) Liu, W.; Wang, G.; Han, D.; Xu, H.; Chu, X. Accurate characterization of coal pore and fissure structure based on CT 3D reconstruction and NMR. *Journal of Natural Gas Science and Engineering* **2021**, *96*. DOI: 104242.

- (3) Liu, P.; Fan, L.; Fan, J.; Zhong, F. Effect of water content on the induced alteration of pore morphology and gas sorption/diffusion kinetics in coal with ultrasound treatment. *Fuel* **2021**, *306*. DOI: 121752.
- (4) Li, Q.; Zhao, Z.; Liu, P.; Nie, B.; Zhao, Y.; Liu, X.; Deng, B.; Wang, M. Evaluation of structural damage and gas transportability change in coal subjected to ultrasound stimulation using image-based modeling and permeability tests. *Fuel* **2023**, *349*. DOI: 128684.
- (5) Wang, Y.; Wang, C.; Gao, S.; Zheng, X.; Darkwa, J. The impact of thermal insulation on cooling energy consumption and optimal insulation thickness for underground tunnel. *Sustainable Energy Technologies and Assessments* **2021**, *47*. DOI: 101495.
- (6) Gao, X.; Qu, Y.; Xiao, Y. A numerical method for cooling and dehumidifying process of air flowing through a deeply buried underground tunnel with unsaturated condensation model. *Applied Thermal Engineering* **2019**, *159*. DOI: 113891.
- (7) Liu, P.; Fan, L.; Li, Q.; Zhong, F. Power ultrasound assisted coalbed methane enhancement recovery: Field application and performance evaluation in underground coal mine. *Fuel* **2022**, *324*. DOI: 124575.
- (8) Lu, X.-x.; Xing, Y.; Shen, C.; Li, Y.-b.; Wang, M.-y.; Liu, J.-p. The characteristic research on the flame retardant of calcification foam on the high temperature coal. *Advanced Powder Technology* **2022**, *33* (1). DOI: 103359.
- (9) Zhang, J.; Ren, T.; Liang, Y.; Wang, Z. A review on numerical solutions to self-heating of coal stockpile: Mechanism, theoretical basis, and variable study. *Fuel* **2016**, *182*, 80–109.
- (10) Wang, H.; Cheng, C.; Chen, C. Characteristics of polycyclic aromatic hydrocarbon release during spontaneous combustion of coal and gangue in the same coal seam. *Journal of Loss Prevention in the Process Industries* **2018**, *55*, 392–399.
- (11) Yuan, L.; Smith, A. C. Numerical study on effects of coal properties on spontaneous heating in longwall gob areas. *Fuel* **2008**, *87* (15–16), 3409–3419.
- (12) Liu, P.; Nie, B.; Zhao, Z.; Li, J.; Yang, H.; Qin, C. Permeability of micro-scale structure in coal: Insights from  $\mu$ -CT image and pore network modelling. *Gas Science and Engineering* **2023**, *111*. DOI: 204931.
- (13) Cheng, W.; Hu, X.; Xie, J.; Zhao, Y. An intelligent gel designed to control the spontaneous combustion of coal: Fire prevention and extinguishing properties. *Fuel* **2017**, *210*, 826–835.
- (14) Deng, J.; Lei, C.; Xiao, Y.; Cao, K.; Ma, L.; Wang, W.; Laiwang, B. Determination and prediction on “three zones” of coal spontaneous combustion in a gob of fully mechanized caving face. *Fuel* **2018**, *211*, 458–470.
- (15) Zheng, Y.; Li, Q.; Zhu, P.; Li, X.; Zhang, G.; Ma, X.; Zhao, Y. Study on Multi-field Evolution and Influencing Factors of Coal Spontaneous Combustion in Goaf. *Combust. Sci. Technol.* **2023**, *195* (2), 247–264.
- (16) Zhang, Y.; Liu, Y.; Shi, X.; Yang, C.; Wang, W.; Li, Y. Risk evaluation of coal spontaneous combustion on the basis of auto-ignition temperature. *Fuel* **2018**, *233*, 68–76.
- (17) Liu, W.; Qin, Y. Multi-physics coupling model of coal spontaneous combustion in longwall gob area based on moving coordinates. *Fuel* **2017**, *188*, 553–566.
- (18) Liu, W.; Zhou, Y.; Chu, X.; Qin, Y.; Hu, J. Effects of seepage behaviors on coal spontaneous combustion in longwall gobs: an investigation between Darcy and non-Darcy seepage. *Fuel* **2022**, *322*. DOI: 124126.
- (19) Song, Y.; Qin, Y.; Yan, L.; Guo, W.; Xu, H. Endothermic relaxation behavior of gangue in longwall gob: Bidirectional heat transfer model and its simulation validation. *Fuel* **2023**, *346*. DOI: 128349.
- (20) Qin, Y.; Yan, L.; Liu, W.; Xu, H.; Song, Y.; Guo, W. Continuous monitoring system of gob temperature and its application. *Environ. Sci. Pollut. Res. Int.* **2022**, *29* (35), 53063–53075.
- (21) Liu, W.; Qin, Y.; Shi, C.; Guo, D. Dynamic evolution of spontaneous combustion of coal in longwall gobs during mining-stopped period. *Process Safety and Environmental Protection* **2019**, *132*, 11–21.
- (22) Feng, G.; Zhang, A.; Hu, S.; Cheng, J.; Miu, X.; Hao, G.; Han, D.; Guan, S.; Zhao, G. A methodology for determining the methane flow space in abandoned mine gobs and its application in methane drainage. *Fuel* **2018**, *227*, 208–217.
- (23) Delgado, J. M. P. Q. Longitudinal and Transverse Dispersion in Porous Media. *Chem. Eng. Res. Des.* **2007**, *85* (9), 1245–1252.
- (24) Bruining, H.; Darwish, M.; Rijnks, A. Computation of the Longitudinal and Transverse Dispersion Coefficient in an Adsorbing Porous Medium Using Homogenization. *Transport in Porous Media* **2012**, *91* (3), 833–859.
- (25) Fel, L.; Bear, R. Dispersion and Dispersivity Tensors in Saturated Porous Media with Uniaxial Symmetry. *Transport in Porous Media* **2010**, *85* (1), 259–268.
- (26) Landman, A. J.; Schotting, R.; Egorov, A.; Demidov, D. Density-dependent dispersion in heterogeneous porous media Part II: Comparison with nonlinear models. *Adv. Water Resources* **2007**, *2481*. DOI: 10.1111/j.1538-7836.2007.02802.x.
- (27) Pourbakhthar, A.; Poulsen, T. G.; Faghihinia, M.; Papadikis, K.; Wilkinson, S. Relating wind-induced gas transport in porous media to wind speed and medium characteristics. *J. Pet. Sci. Eng.* **2020**, *194*, No. 107550.
- (28) Sahimi, M.; Imdakm, A. O. The effect of morphological disorder on hydrodynamic dispersion in flow through porous media. *Journal of Physics A General Physics* **1988**, *21* (19), 3833.
- (29) Ding, h.; Ding, J.; Dong, X. Phosphogypsum Yard Leakage Pollution Prediction and Seepage Prevention of Guizhou Longjingwan. *J. Guizhou Univ.* **2016**, *33* (5), 5.
- (30) Zhang, M.; Zeng, Z.; Gao, H.; Wu, K. Two-Dimensional Dispersion Experiment in Laboratory. *J. Lanzhou Univ.* **1993**, *29* (4), 5.
- (31) Romero-Gomez, P.; Li, Z.; Choi, C. Y.; Buchberger, S. G. Axial Dispersion Coefficients for Laminar Flows in Water Distribution Systems. *World Environ. Water Resources Congress* **2009**, *2009*, 1–10.
- (32) Jiao, C. Y.; Hötzl, H. An Experimental Study of Miscible Displacements in Porous Media with Variation of Fluid Density and Viscosity. *Transport in Porous Media* **2004**, *54* (2), 125–144.
- (33) Pugliese, L.; Poulsen, T. G. Estimating Solute Dispersion Coefficients in Porous Media at Low Pore Water Velocities. *Soil Science* **2014**, *179* (4), 175–181.
- (34) Xu, H.; Qin, Y.; Wu, F.; Zhang, F.; Liu, W.; Liu, J.; Guo, M. Numerical modeling of gas extraction from coal seam combined with a dual-porosity model: Finite difference solution and multi-factor analysis. *Fuel* **2022**, *313*. DOI: 122687.
- (35) Zhang, F.; Liu, W.; Qin, Y.; Chu, X.; Xu, H.; Wu, F.; Li, Y. Optimization of coalbed methane recovery from extraction borehole using novel plastic spraying material: A field application and evaluation. *Process Safety and Environmental Protection* **2023**, *169*, 534–546.
- (36) Delgado, J. M. P. Q. A critical review of dispersion in packed beds. *Heat and Mass Transfer* **2006**, *42* (4), 279–310.
- (37) Liu, W.; Chu, X.; Qi, M.; Han, D.; Zhang, S.; Qin, Y. Adsorption and diffusion behavior of two-component gases in coal particles at different temperatures. *Fuel* **2023**, *339*. DOI: 126899.
- (38) Liu, P.; Liu, A.; Liu, S.; Qi, L. Experimental evaluation of ultrasound treatment induced pore structure and gas desorption behavior alterations of coal. *Fuel* **2022**, *307*, No. 121855.
- (39) Dzmitry; Hlushkou; Stanislaw; Piatruszka; Ulrich; Tallarek. Impact of diffusion on transverse dispersion in two-dimensional ordered and random porous media. *Phys. Rev. E* **2017**, *95* (6), No. 063108, DOI: 10.1103/physreve.95.063108.
- (40) Zheng, J. I. A. Y. I.; Shi, X. I. N. G.; Shi, J. U. A. N.; Chen, Z. H. E. N. Q. I. A. N. Pore structure reconstruction and moisture migration in porous media. *Fractals* **2014**, *22* (03), 1440007.
- (41) Liu, W.; Song, H.; Li, X. Dimensionless analysis on gas emission law around tunneling face. *J. China Coal Soc.* **2015**, *40*, 151. DOI: 10.13225/j.cnki.jccs.2014.3024.
- (42) Song, H.; Chen, Q. Dimensionless analysis of soil temperature field of shallow subway tunnel. *Energy and Buildings* **2022**, *259*. DOI: 111900.

- (43) Liu, W.; Chu, X.; Han, D.; Chen, W.; Qin, Y.; Guo, W. Dimensionless prejudgment criterion of coal spontaneous combustion in longwall gobs and its application. *Fuel* **2023**, 353. DOI: 129174.
- (44) Sağıroğlu, A.; Karagöz, İ.; Özcan, Ö. Ö.; Ergüzel, T. T.; Karahan, M.; Tarhan, N. Evaluation of the glioblastoma multiforme treatment with hyperthermia using the finite element method. *Numer. Heat Transfer, Part A* **2022**, 1–22.
- (45) Liu, W.; Liang, S.; Shi, C. Risk modelling and simulation of thermal safety in underground railway tunnel surrounding. *Accid Anal Prev* **2022**, 168, No. 106620.
- (46) Jiayi, Z.; Xing, S.; Juan, S.; Zhenqian, C. Finite volume hydromechanical simulation in porous media. *Water Resour. Res.* **2014**, 22, 4379 DOI: [10.1142/S0218348X14400076](https://doi.org/10.1142/S0218348X14400076).
- (47) Cai, Y.; Zhang, Y.; Qi, Q.; Qin, Y.; Zhou, T.; Sun, Z. Optimization of Numerical Simulation Algorithm for Spontaneous Combustion in Goaf via a Compression Storage and Solution Method of Coefficient Matrix. *Fire* **2022**, 5 (3), 71.
- (48) Qin, Y.; Li, Y.; Zhao, Y.; Xu, H.; Liu, H.; Zhao, J.; Xu, J. Study on gas transport behavior in coal matrix based on free gas density gradient diffusion: Comparison with fick model. *Gas Science and Engineering* **2023**, 111. DOI: 204914.
- (49) Xu, H.; Qin, Y.; Yang, D.; Zhang, F.; Wu, F.; Chu, X. Modeling of diffusion kinetics during gas adsorption in a coal seam with a dimensionless inversion method. *Fuel* **2022**, 326. DOI: 125068.